**Supplementary Information to:**

# Holocene temperatures in southwestern Greenland controlled by topography, ice sheet proximity and oceanic conditions

Sudip Acharya[1,*], Allison A. Cluett[1,2], Amy L. Grogan[1], Jason P. Briner[1], Isla S. Castañeda[3], Elizabeth K Thomas[1]

[1] Department of Geology, State University of New York at Buffalo, Buffalo, NY, USA

[2] University of California, Santa Cruz and NOAA Southwest Fisheries Science Center

[3] University of Massachusetts Amherst, Amherst, MA, USA

[*] Correspondence to: Sudip Acharya (sudip.ach@buffalo.edu)

**Supplementary Figures:**

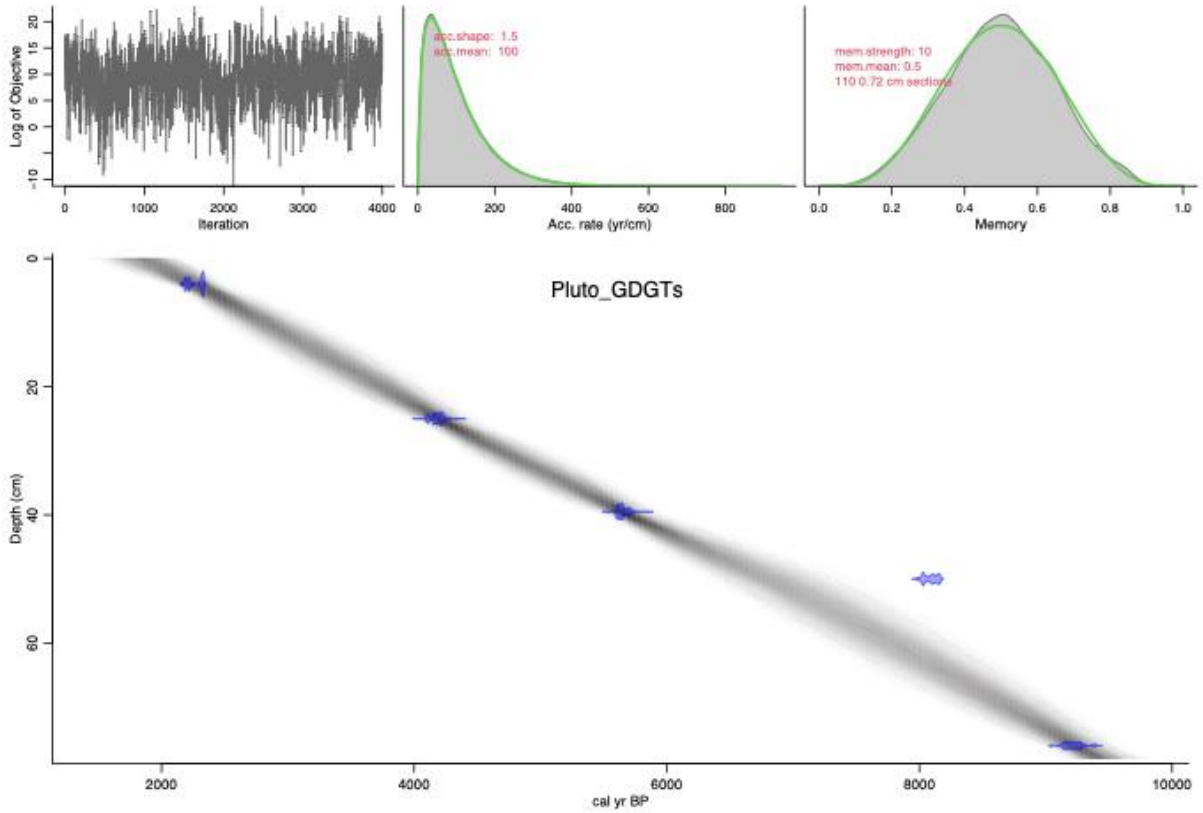


**Figure S1:** Age-depth model for the sediment core from Pluto lake. Age depth model is based on five radiocarbon ages from aquatic macrofossils (Thomas et al., 2020), generated using geochronr package (Blaauw & Christen, 2011; McKay et al., 2021). Blue symbols indicate calibrated ratiocarbon ages using IntCal20 (Reimer et al., 2020). Gray shadding indicates the 95% confidence interval for the generated age-depth model.

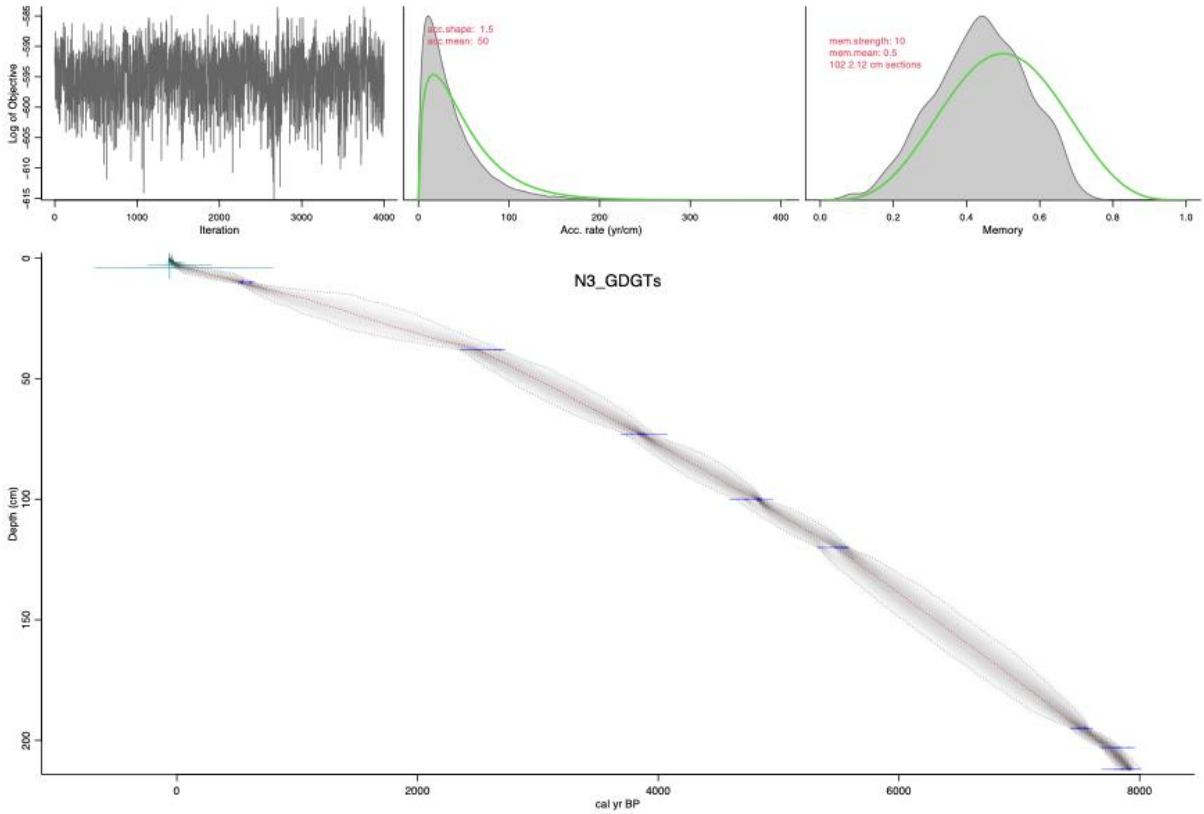


**Figure S2:** Age-depth model for the sediment core from N3 lake. Age depth model is based on eight radiocarbon ages from aquatic macrofossils (Blue symbols) and $^{210}$Pb ages (green symbols) for upper 4 cm (Thomas et al., 2016), generated using geochronr package (Blaauw & Christen, 2011; McKay et al., 2021). Blue symbols indicate calibrated ratiocarbon ages using IntCal20 (Reimer et al., 2020). Green symbols indicate the $^{210}$Pb ages. Gray shadding indicates the 95% confidence interval for the generated age-depth model. Please refer to (Thomas et al., 2016) for detailed age-depth model description.

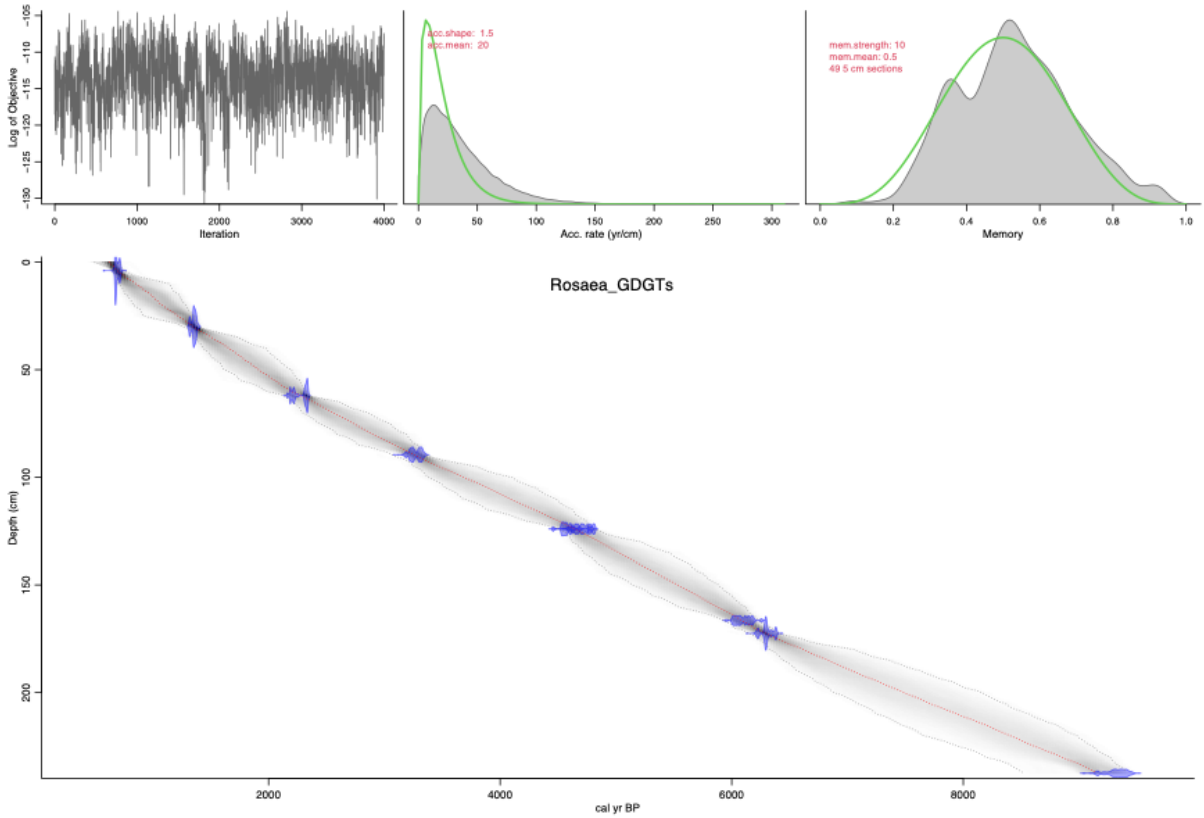


**Figure S3:** Age-depth model for the sediment core from Rosaea lake. Age depth model is based on eight radiocarbon ages from aquatic macrofossils, generated using geochronr package (Blaauw & Christen, 2011; McKay et al., 2021). Blue symbols indicate calibrated ratiocarbon ages using IntCal20 (Reimer et al., 2020). Gray shadding indicates the 95% confidence interval for the generated age-depth model.

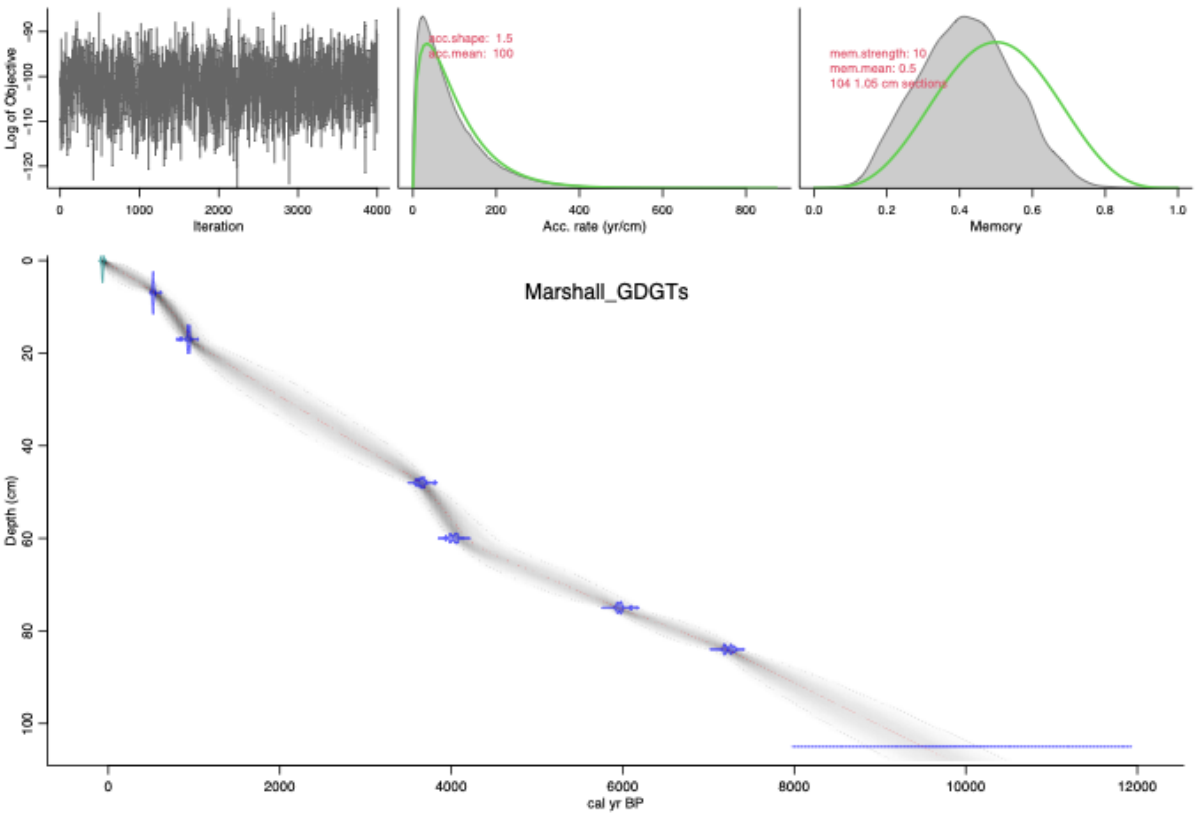


**Figure S4:** Age-depth model for the sediment core from Marshall lake. Age depth model is based on seven radiocarbon ages from aquatic macrofossils, generated using geochronr package (Blaauw & Christen, 2011; McKay et al., 2021). Blue symbols indicate calibrated ratiocarbon ages using IntCal20 (Reimer et al., 2020). Green symbol indicate the year of core collection. Gray shadding indicates the 95% confidence interval for the generated age-depth model.

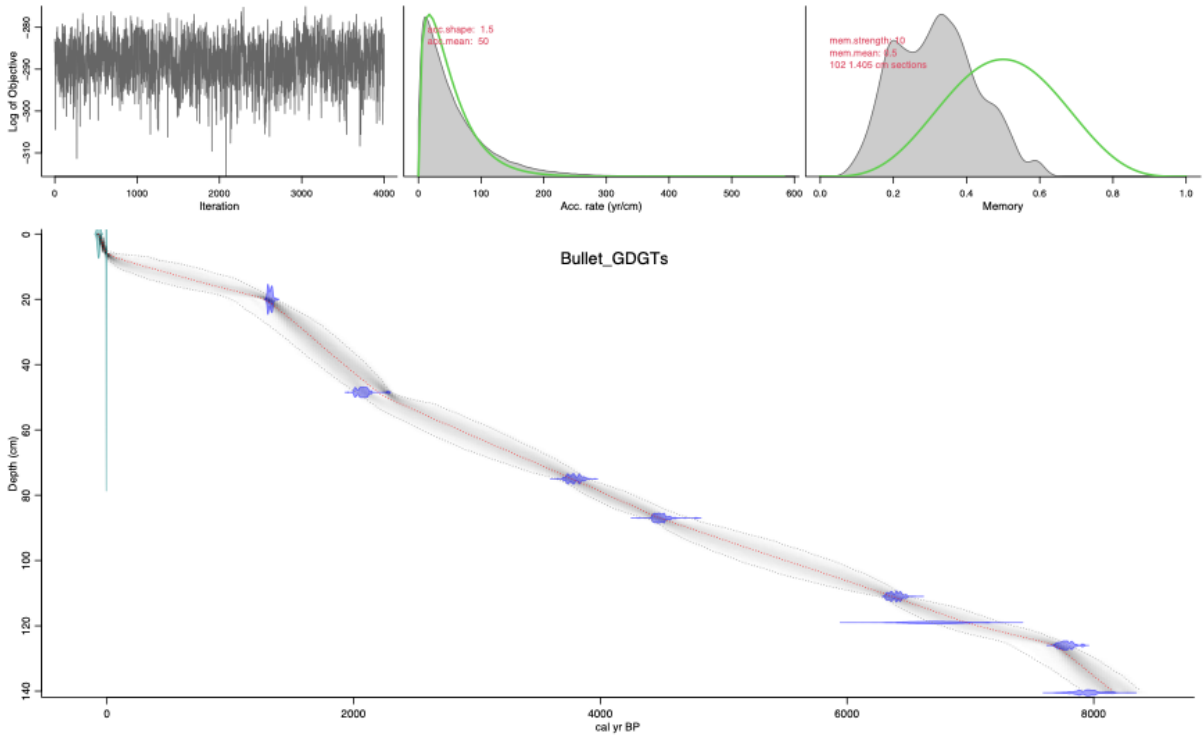


**Figure S5:** Age-depth model for the sediment core from Bullet lake. Age depth model is based on eight radiocarbon ages from aquatic macrofossils, generated using geochronr package (Blaauw & Christen, 2011; McKay et al., 2021). Blue symbols indicate calibrated ratiocarbon ages using IntCal20 (Reimer et al., 2020). Green symbol at 0 cm depth indicates the year of core collection and at 5 cm indicates the calibrated age using Northern Hemisphere Zone 1 compilation (Hua et al., 2013). Gray shadding indicates the 95% confidence interval for the generated age-depth model.

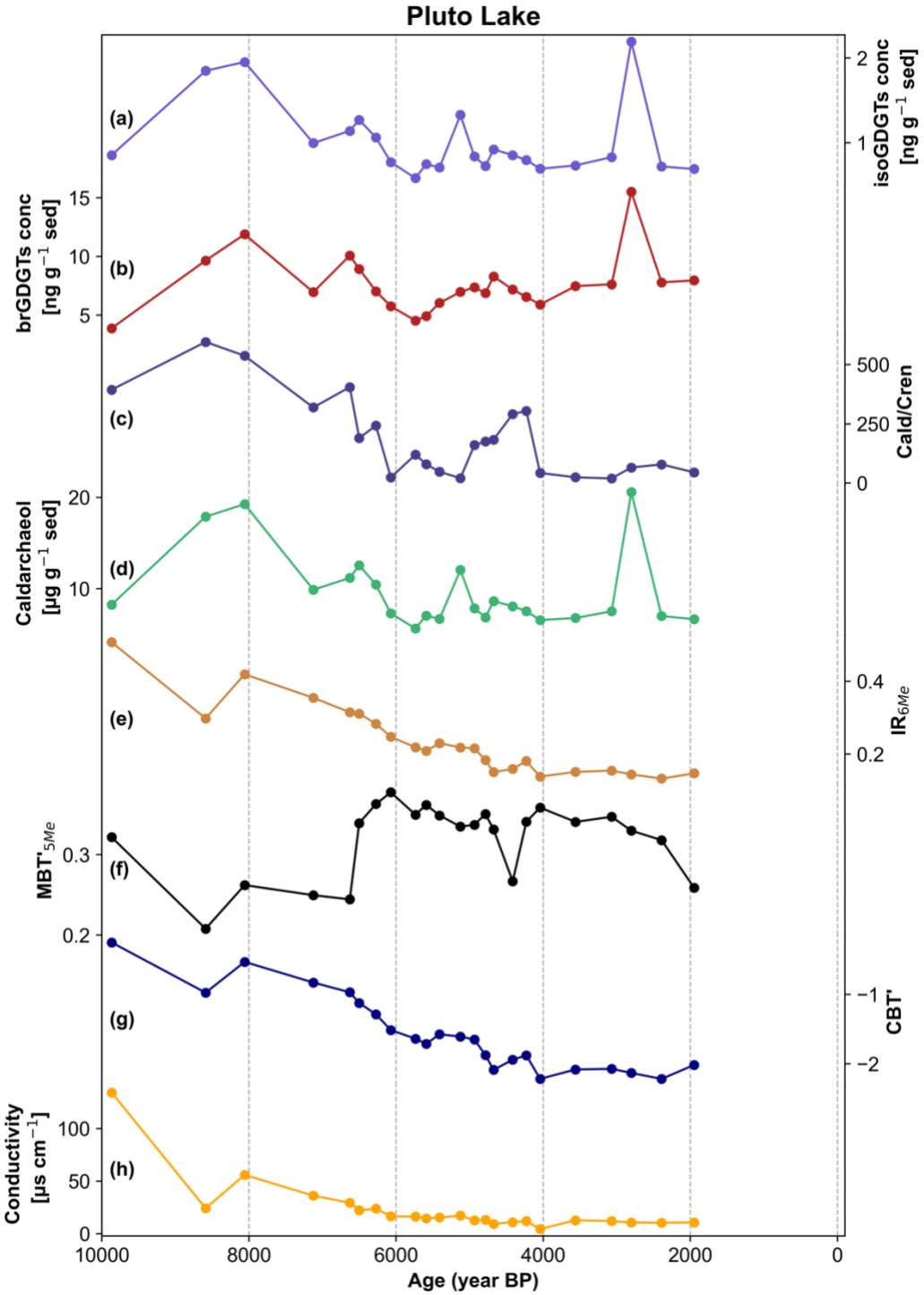


**Figure S6:** The downcore pattern of GDGTs and their indices in Lake Pluto sediments. (a) Isoprenoid (iso) GDGTs concentration in ng $g^{-1}$ of dry sediment [ng $g^{-1}$ sed], (b) branched (br) GDGTs concentration in ng $g^{-1}$ of dry sediment [ng $g^{-1}$ sed], (c) ratio of Caldarcharol to Crenarchaeol (Clad/Cren), (d) concentraiton of Caldarcharol in µg $g^{-1}$ of dry sediment [µg $g^{-1}$ sed], (e) isomerization ratio ($IR_{6ME}$), (f) methylation of branched tetraethers ($MBT'_{5Me}$), (g) cyclization of branched tetraethers (CBT′), and (h) conductivity [µs $cm^{-1}$].

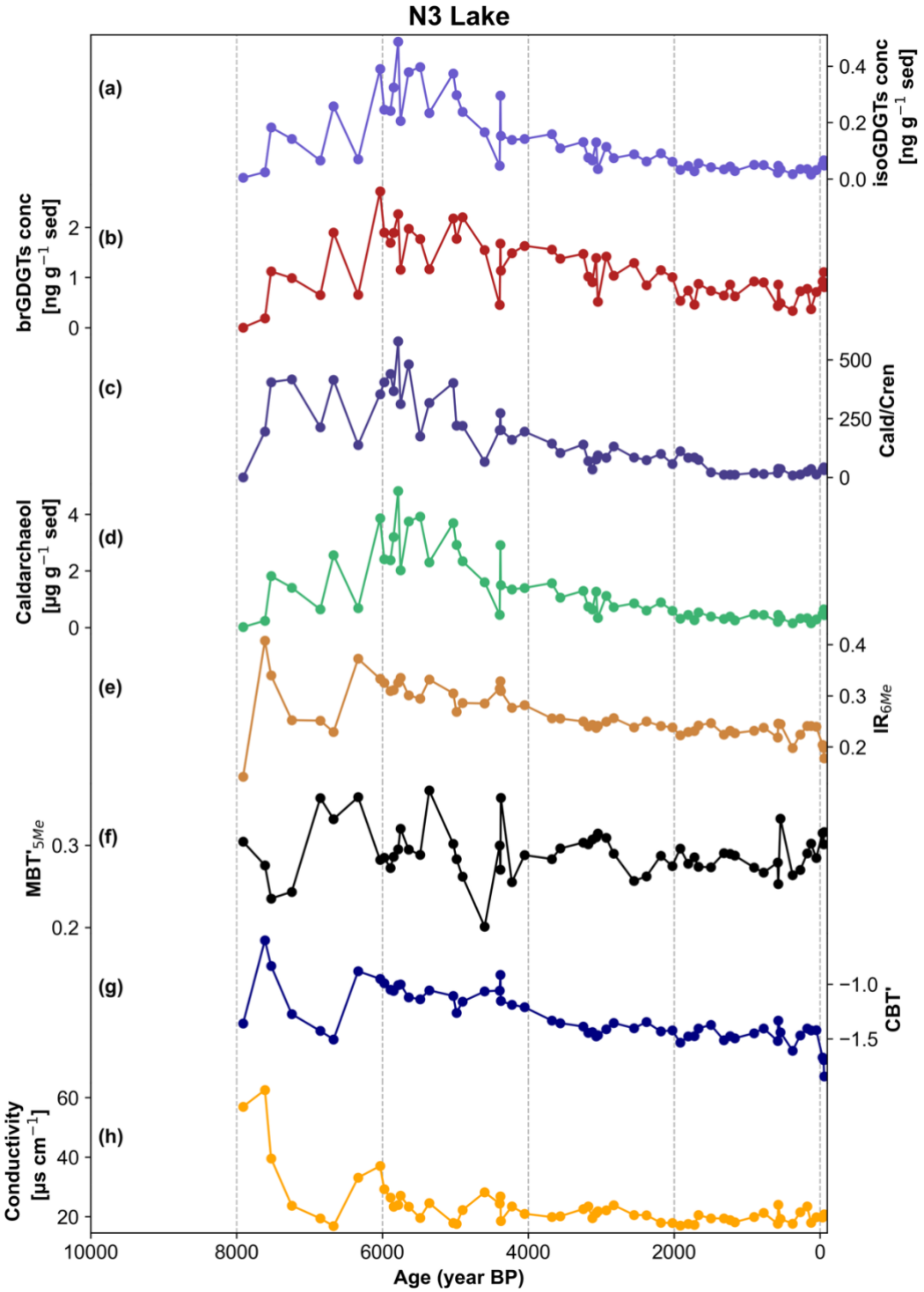


**Figure S7:** The downcore pattern of GDGTs and their indices in Lake N3 sediments. (a) Isoprenoid (iso) GDGTs concentration in ng $g^{-1}$ of dry sediment [ng $g^{-1}$ sed], (b) branched (br) GDGTs concentration in ng $g^{-1}$ of dry sediment [ng $g^{-1}$ sed], (c) ratio of Caldarcharol to Crenarchaeol (Clad/Cren), (d) concentraiton of Caldarcharol in µg $g^{-1}$ of dry sediment [µg $g^{-1}$ sed], (e) isomerization ratio ($IR_{6ME}$), (f) methylation of branched tetraethers ($MBT'_{5Me}$), (g) cyclization of branched tetraethers (CBT′), and (h) conductivity [µs $cm^{-1}$].

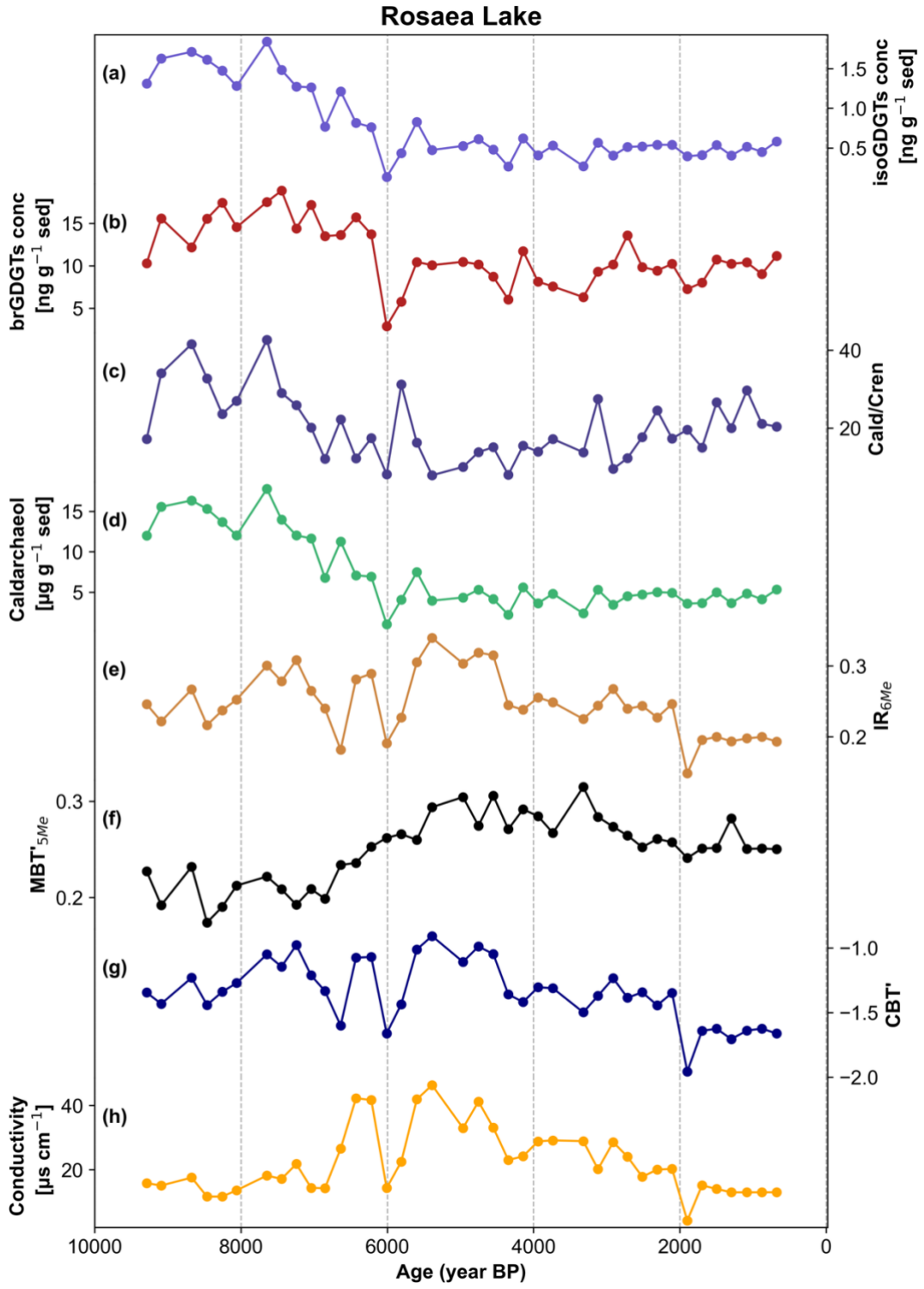


**Figure S8:** The downcore pattern of GDGTs and their indices in Lake Rosaea sediments. (a) Isoprenoid (iso) GDGTs concentration in ng $g^{-1}$ of dry sediment [ng $g^{-1}$ sed], (b) branched (br) GDGTs concentration in ng $g^{-1}$ of dry sediment [ng $g^{-1}$ sed], (c) ratio of Caldarcharol to Crenarchaeol (Clad/Cren), (d) concentraiton of Caldarcharol in µg $g^{-1}$ of dry sediment [µg $g^{-1}$ sed], (e) isomerization ratio ($IR_{6ME}$), (f) methylation of branched tetraethers ($MBT'_{5Me}$), (g) cyclization of branched tetraethers (CBT′), and (h) conductivity [µs $cm^{-1}$].

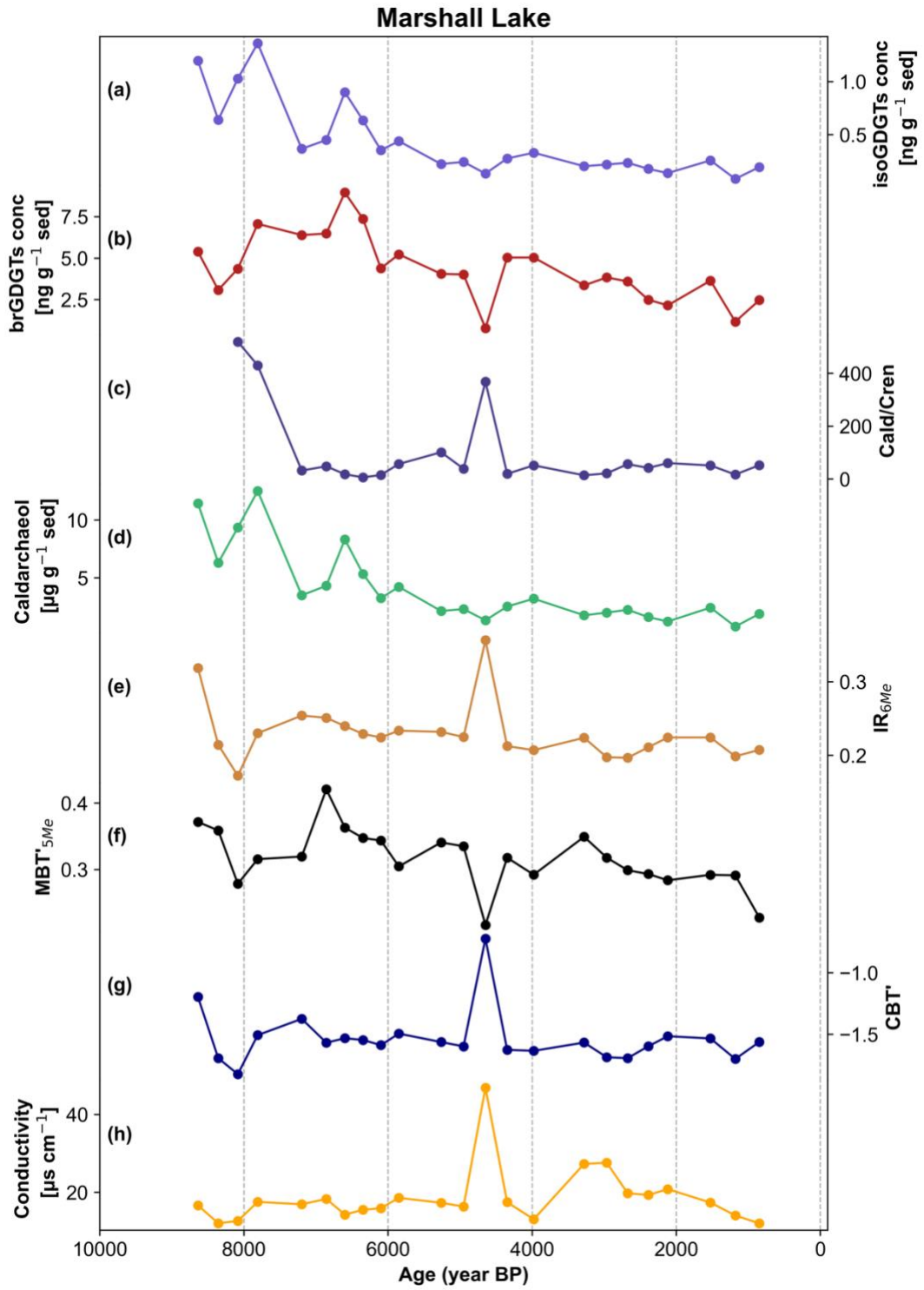


**Figure S9:** The downcore pattern of GDGTs and their indices in Lake Marshall sediments. (a) Isoprenoid (iso) GDGTs concentration in ng $g^{-1}$ of dry sediment [ng $g^{-1}$ sed], (b) branched (br) GDGTs concentration in ng $g^{-1}$ of dry sediment [ng $g^{-1}$ sed], (c) ratio of Caldarcharol to Crenarchaeol (Clad/Cren), (d) concentraiton of Caldarcharol in µg $g^{-1}$ of dry sediment [µg $g^{-1}$ sed], (e) isomerization ratio ($IR_{6ME}$), (f) methylation of branched tetraethers ($MBT'_{5Me}$), (g) cyclization of branched tetraethers (CBT′), and (h) conductivity [µs $cm^{-1}$].

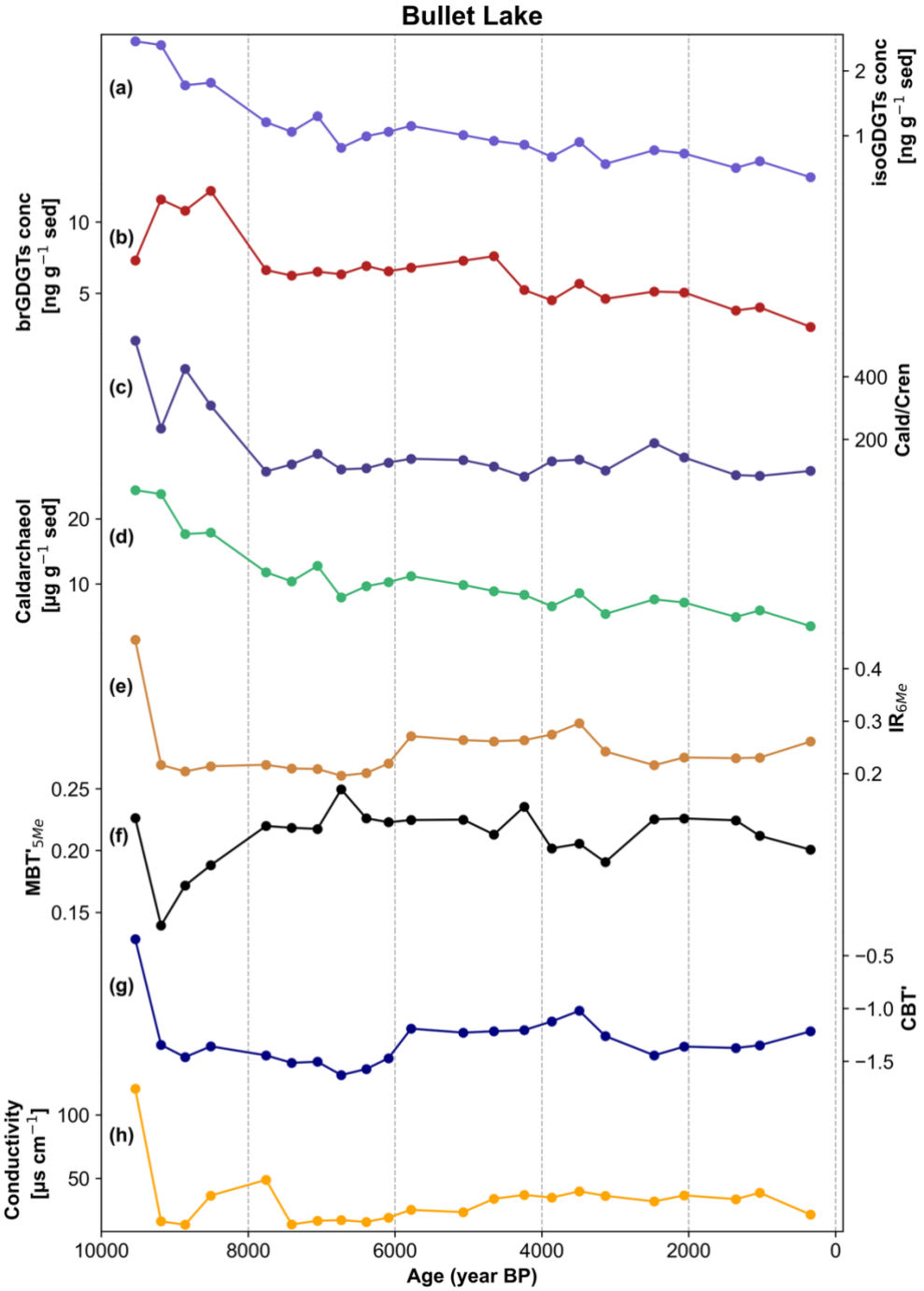


**Figure S10:** The downcore pattern of GDGTs and their indices in Lake Bullet sediments. (a) Isoprenoid (iso) GDGTs concentration in ng $g^{-1}$ of dry sediment [ng $g^{-1}$ sed], (b) branched (br) GDGTs concentration in ng $g^{-1}$ of dry sediment [ng $g^{-1}$ sed], (c) ratio of Caldarcharol to Crenarchaeol (Clad/Cren), (d) concentraiton of Caldarcharol in µg $g^{-1}$ of dry sediment [µg $g^{-1}$ sed], (e) isomerization ratio ($IR_{6ME}$), (f) methylation of branched tetraethers ($MBT'_{5Me}$), (g) cyclization of branched tetraethers (CBT′), and (h) conductivity [µs $cm^{-1}$].

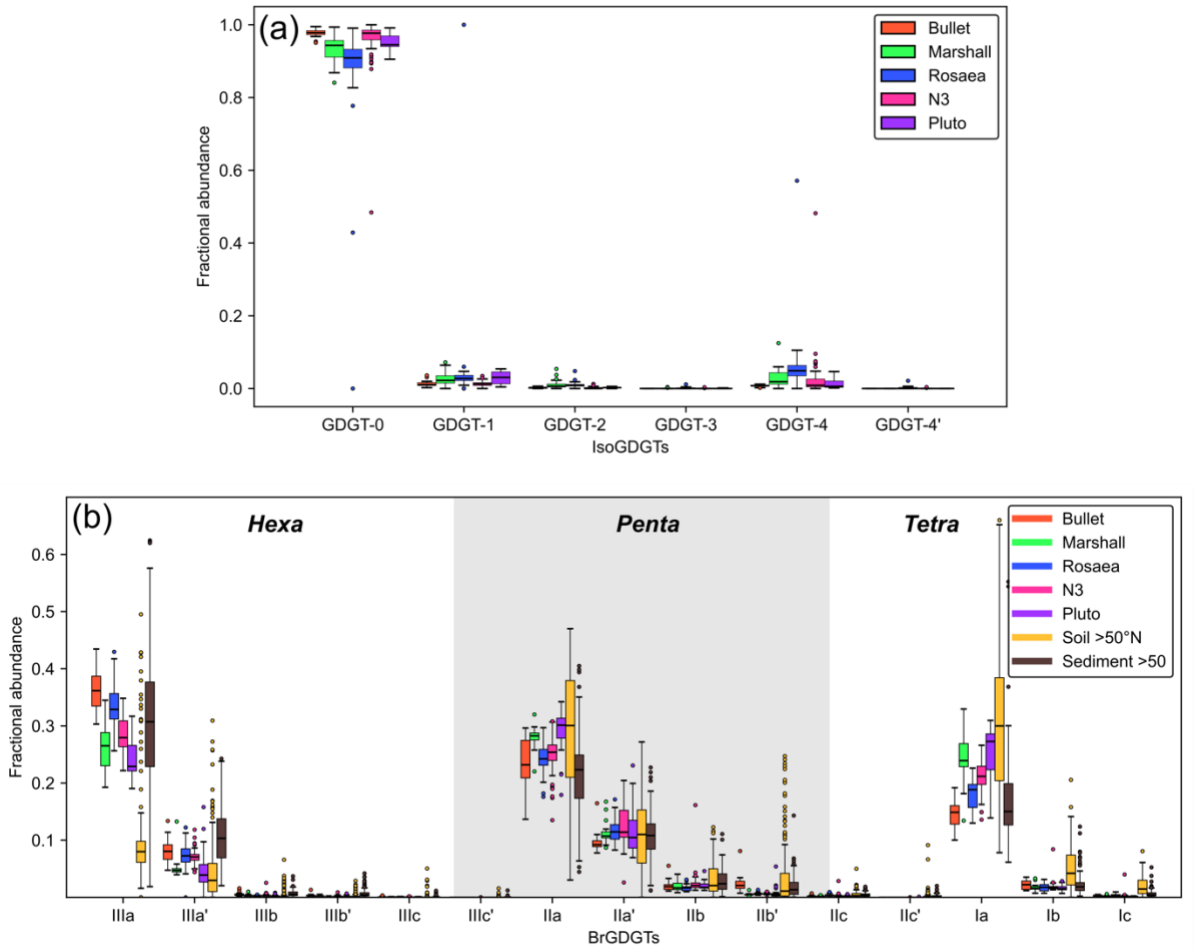


**Figure S11:** (a) Fractional abundance of isoGDGTs. (b) Comparison of fractional abundance of brGDGTs from southwestern Greenland lakes with high latitude (>50°N) soil and lake sediment samples.

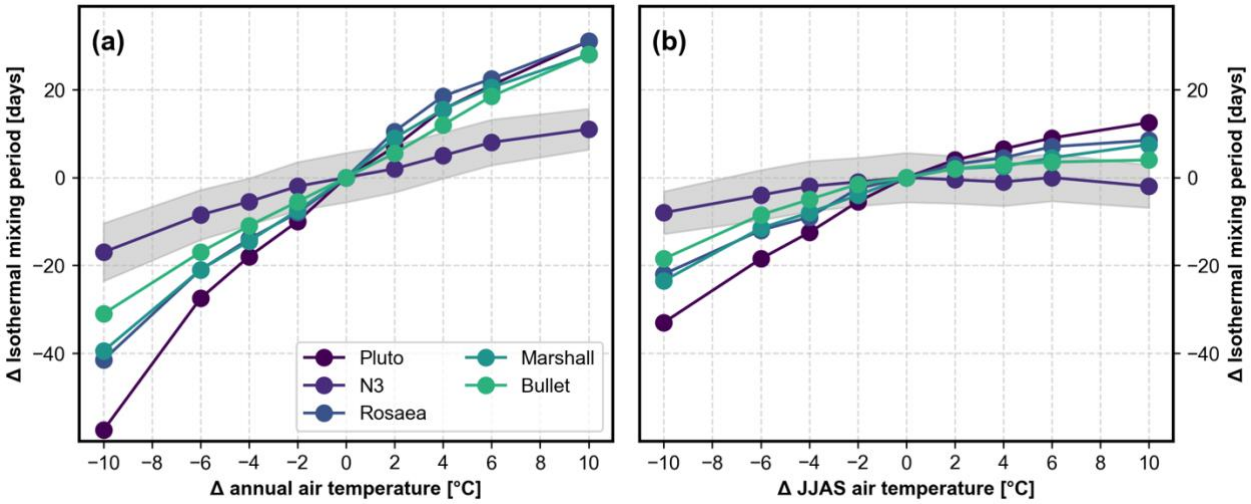


**Figure S12:** Sensitivity of the isothermal mixing period [days] in studied lakes to changes in (a) annual air temperature and (b) JJAS air temperature. Higher air temperature generally causes prolonged isothermal mixing (i.e., reduced duration of stratification) during the ice-free season, and vice versa for colder conditions. Each point denotes the median value of the 30 year model run average. Gray shading represents the standard deviation for the 30 years of model runs for Lake N3. Standard derivation shows minor variation between lakes.

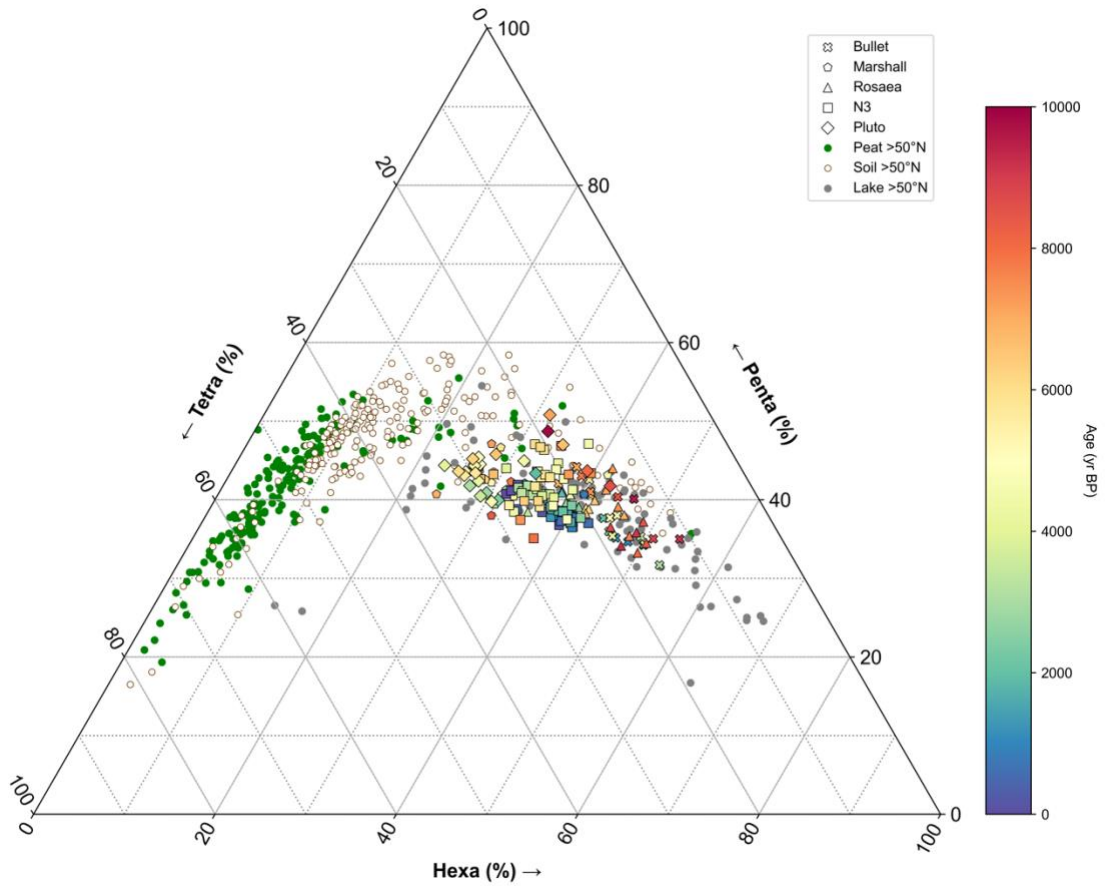


**Figure S13:** Ternary diagram showing the fractional abundance of hexa, penta and tetra methylated brGDGTs with high latitude (>50°N) soil, lake sediment and peat samples.

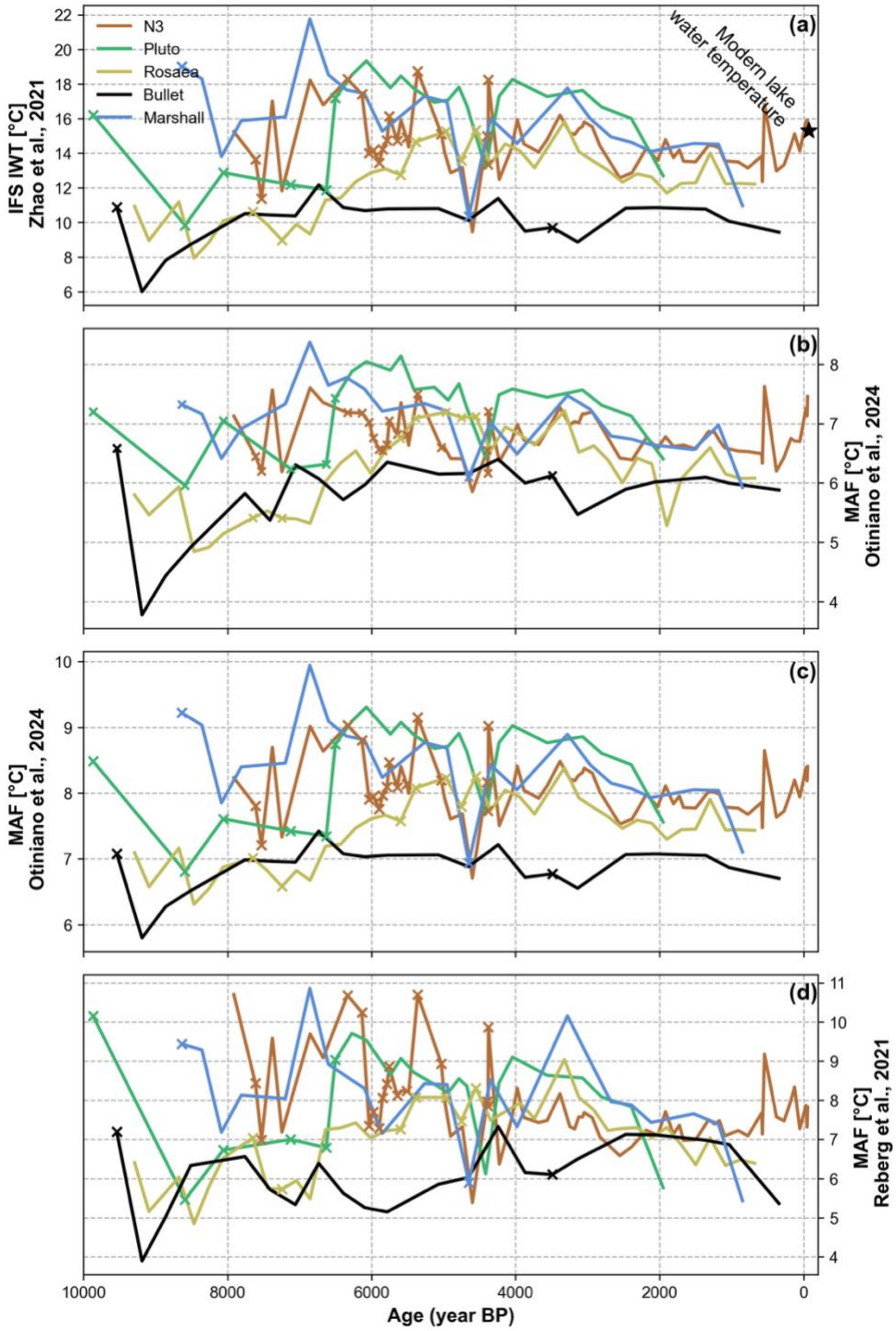


**Figure S14:** Reconstructed Holocene temperatures in southwestern Greenland lakes using (a) Zhao et al., (2021), (b) Otiniano et al., (2024), (c) Otiniano et al., (2023), and (d) Raberg et al., (2021) calibrations. Samples with $IR_{6ME}$>0.3, which are interpreted to be affected by non thermal effect on brGDGTs, are indicated by X. Black star symbol in (a) indicates the the moden July lake water temperature from N3 lake. ISF LWT represents ice free season lake water tempeature and MAF represents mean air temperate above freezing.

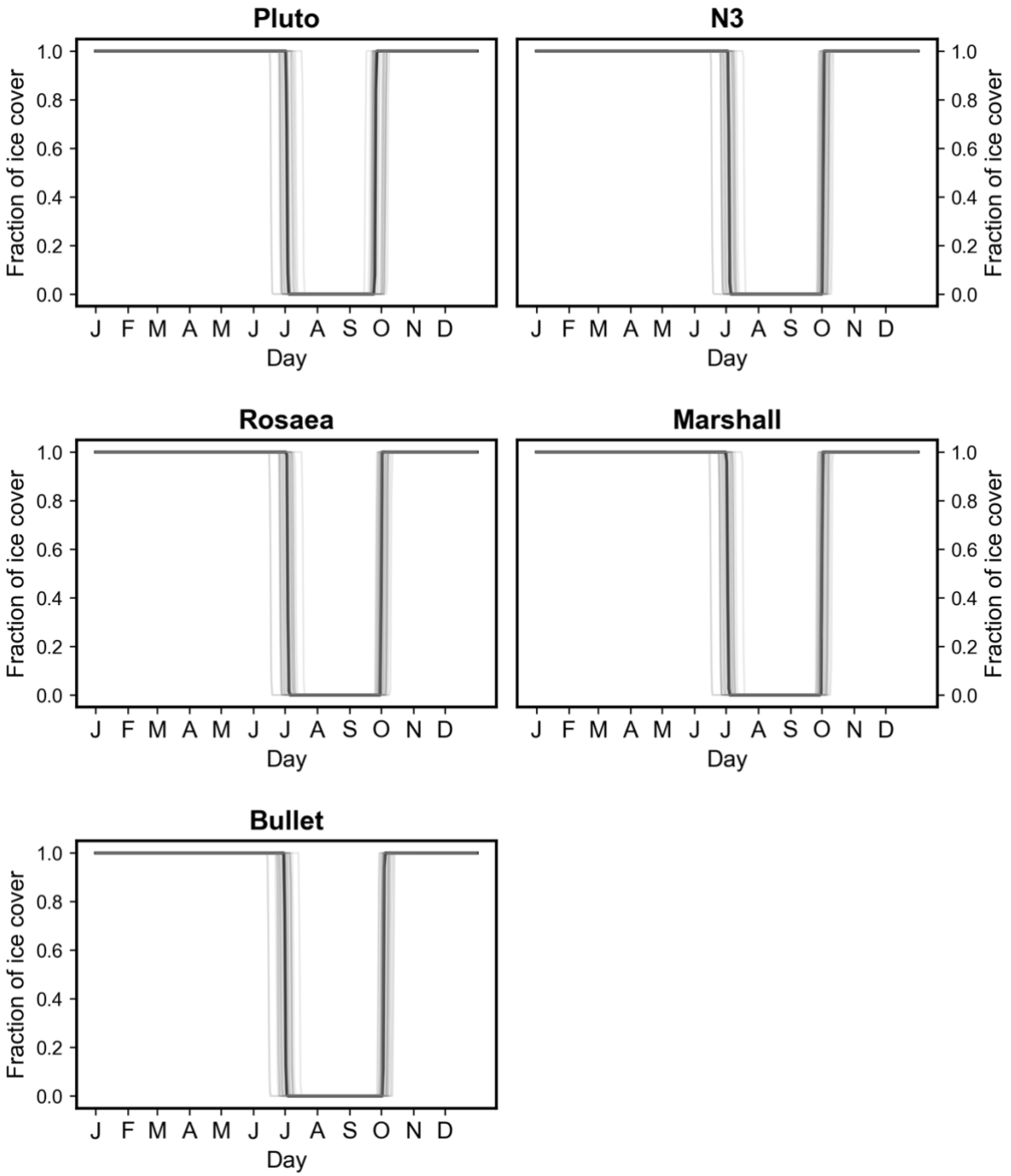


**Figure S15:** Simulated fraction of ice cover in study lakes. The black line indicates the median fraction of ice cover for 30 years of model runs, while the gray line shows the fraction of ice cover for each year of model run. A fraction of ice cover value of 1 indicates fully ice cover, while 0 indicates completely open.

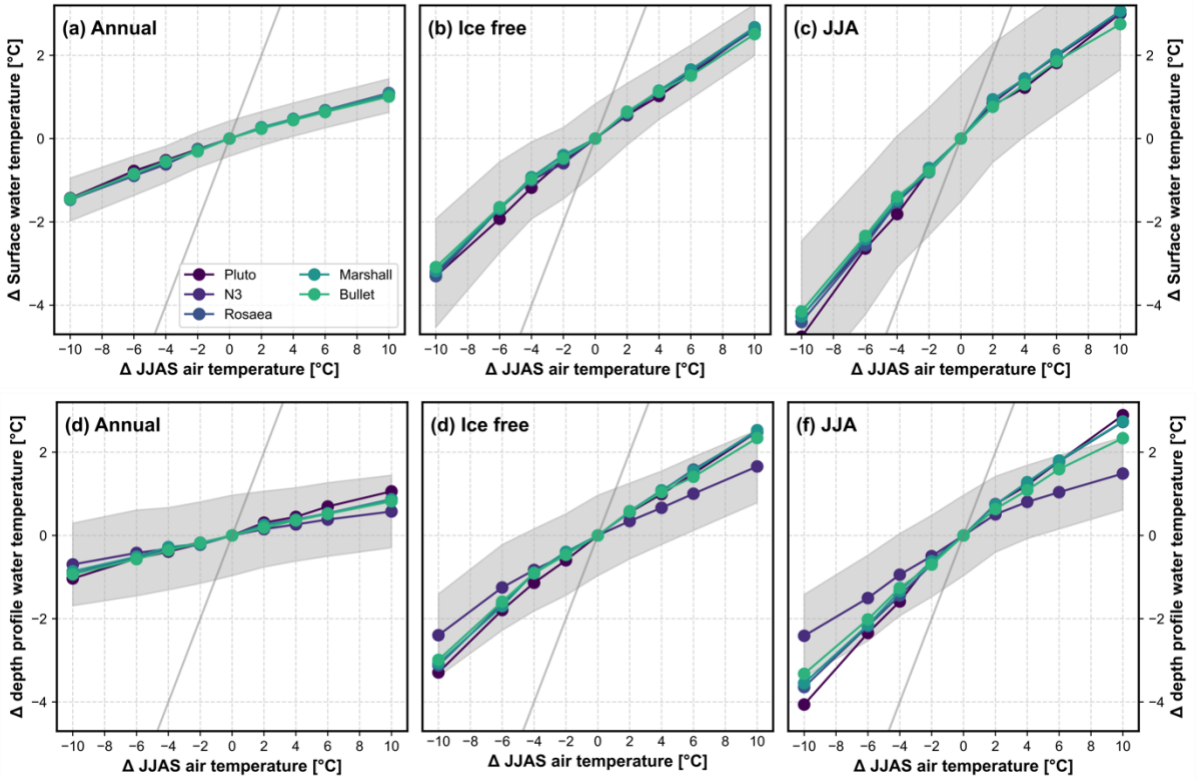


**Figure S16:** Sensitivity of average surface water and depth profile temperatures to changes in JJAS air temperature. Changes in (A) annual (B) ice free and (C) JJA surface water temperature [°C], with changes in JJAS air temperature. Changes in (D) annual (E) ice free and (F) JJA average depth profile water temperature [°C], with changes in JJAS air temperature. Gray lines indicate the 1:1 line. Gray shading represents the standard deviation of 30 years of model runs for Lake N3. Standard derivation is on the same order for other lakes.

155
156 **Supplementary tables:**
157 **Table S1.** The $^{14}C$ calculation parameters, radiocarbon ages and 2σ calibrated ages
158 for the sediment core from Lake Marshall. All$^{14}C$-ages were calibrated using IntCal20
159 calibration dataset (Reimer et al., 2020).

| Accession # | Core | Top depth (cm) | Sample thickness (cm) | Sample material | $F^{14}C$ modern | Fm err | $\delta^{13}C$ (‰) | $^{14}C$age and uncertainty (yr) | Median calibrated age (yr BP) and 2σ uncertainty (yr) |
|---|---|---|---|---|---|---|---|---|---|
| OS-138405 | 17Mar-C1 | 7 | 1 | Aquatic macrofossils | 0.8049 | 0.0017 | -24.34 | 495 ± 20 | 523 ± 17 |
| OS-144352 | 17Mar-C1 | 16.5 | 0.5 | Aquatic macrofossils | 0.8804 | 0.0019 | -22.48 | 1020 ± 20 | 936 ± 21 |
| OS-144353 | 17Mar-C1 | 48 | 1 | Aquatic macrofossils | 0.6541 | 0.0016 | -25.93 | 3410 ± 20 | 3648 ± 119 |
| OS-151282 | 17Mar-C1 | 60 | 1.5 | Aquatic macrofossils | 0.6321 | 0.0017 | -28.72 | 3680 ± 20 | 4035 ± 81 |
| OS-151378 | 17Mar-C1 | 73 | 1.5 | Aquatic macrofossils | 0.5229 | 0.0018 | -27.81 | 5210 ± 30 | 5966 ± 126 |
| OS-144354 | 17Mar-C1 | 83.5 | 0.5 | Aquatic macrofossils | 0.4550 | 0.0018 | -27.37 | 6330 ± 30 | 7251 ± 76 |
| OS-137548 | 17Mar-C1 | 104.5 | 0.5 | Aquatic macrofossils | 0.37700 | 0.007 | -27.3 | 8692 ± 331 | 9763 ± 932 |

160
161
162

**Table S2.** The $^{14}C$ calculation parameters, radiocarbon ages, and 2σ calibrated ages for the sediment core from Bullet Lake.

| Accession # | Core | Top depth (cm) | Sample thickness (cm) | Sample material | $F^{14}C$ modern | Fm err | $\delta^{13}C$ (‰) | $^{14}C$age and uncertainty (yr) | Median calibrated age (yr BP) and 2σ uncertainty (yr) |
|---|---|---|---|---|---|---|---|---|---|
| OS-144491 | 17BLT-A1a | 5.25 | 0.5 | Aquatic macrofossils | 1.0061 | 0.0024 | -23.92 | -5 ± 1 | -5 ± 1* |
| OS-151280 | 17BLT-A1a | 20 | 0.5 | Aquatic macrofossils | 0.8383 | 0.0019 | -25.74 | 1420 ± 20 | 1324 ± 26 |
| OS-144350 | 17BLT-A1a | 48.5 | 0.5 | Aquatic macrofossils | 0.7691 | 0.0020 | -26.68 | 2110 ± 20 | 2071 ± 72 |
| OS-151376 | 17BLT-A1b | 75 | 0.5 | Aquatic macrofossils | 0.6450 | 0.0021 | -28.61 | 3520 ± 25 | 3781 ± 90 |
| OS-144351 | 17BLT-A1b | 87 | 4 | Aquatic macrofossils | 0.6064 | 0.0021 | -29 | 4020 ± 30 | 4479 ± 77 |
| OS-151281 | 17BLT-A1b | 111 | 0.5 | Aquatic macrofossils | 0.4969 | 0.0017 | -29.23 | 5620 ± 20 | 6393 ± 87 |
| OS-151370 | 17BLT-A1b | 119 | 0.5 | Aquatic macrofossils | 0.4802 | 0.0081 | -25.72 | 5890 ± 140 | 6715 ± 381 |
| OS-144131 | 17BLT-A1b | 126 | 0.7 | Aquatic macrofossils | 0.4212 | 0.0017 | -26.73 | 6950 ± 30 | 7773 ± 114 |
| OS-151377 | 17BLT-A1b | 140.5 | 0.5 | Aquatic macrofossils | 0.4117 | 0.0041 | -25.4 | 7130 ± 80 | 7949 ± 193 |

*Indicates a $^{14}C$-age calibrated with the bomb peak Northern Hemisphere 1 calibration dataset (Hua et al., 2013). Rest of the $^{14}C$-ages were calibrated using IntCal20 calibration dataset (Reimer et al., 2020).

**Table S3.** The $^{14}C$ calculation parameters, radiocarbon ages, and 2σ calibrated ages for the sediment core from Rosaea Lake. All$^{14}C$-ages were calibrated using IntCal20 calibration dataset (Reimer et al., 2020).

| LabID | Core | Top depth (cm) | Sample thickness (cm) | Sample material | $F^{14}C$ modern | Fm err | $\delta^{13}C$ (‰) | $^{14}C$-age and uncertainty (year) | Median calibrated age (yr BP) and 2σ uncertainty |
|---|---|---|---|---|---|---|---|---|---|
| OS-147583 | 18ROS-A2a | 4 | 0.5 | Aquatic macrofossils | 0.9097 | 0.0020 | -28.0 | 760 ± 20 | 683 ± 20 |
| OS-147584 | 18ROS-A2a | 30 | 0.5 | Aquatic macrofossils | 0.8321 | 0.0017 | -24.79 | 1480 ± 15 | 1359 ± 20 |
| OS-151277 | 18ROS-A2a | 62 | 0.5 | Aquatic macrofossils | 0.7525 | 0.0019 | -28.22 | 2280 ± 20 | 2321 ± 20 |
| OS-151278 | 18ROS-A2a | 89.5 | 0.5 | Aquatic macrofossils | 0.6843 | 0.0016 | -27.29 | 3050 ± 20 | 3264 ± 20 |
| OS-151279 | 18ROS-A2b | 124 | 0.5 | Aquatic macrofossils | 0.6009 | 0.0016 | -24.5 | 4090 ± 20 | 4579 ± 20 |
| OS-147585 | 18ROS-A2b | 124 | 0.5 | Aquatic macrofossils | 0.5955 | 0.0015 | -28.34 | 4160 ± 20 | 4706 ± 20 |
| OS-151375 | 18ROS-A2b | 166.5 | 0.5 | Aquatic macrofossils | 0.5158 | 0.0018 | -26.9 | 5320 ± 30 | 6089 ± 20 |
| OS-151136 | 18ROS-A2b | 172.5 | 0.5 | Aquatic macrofossils | 0.5041 | 0.0017 | -25.83 | 5500 ± 30 | 6297 ± 20 |
| OS-144356 | 18ROS-A2b | 237.5 | 0.5 | Aquatic macrofossils | 0.3551 | 0.0019 | -23.44 | 8320 ± 45 | 9342 ± 20 |